2014-05

Common-Reflection-Point Migration Velocity Analysis of 2D P-Wave Data From TTI Media

UTD AUTHOR(S): Ernesto V. Oropeza and George A. McMechan

GEOPHYSICS, VOL. 79, NO. 3 (MAY-JUNE 2014); P. C65–C79, 16 FIGS.
10.1190/GEO2013-0295.1

Common-reflection-point migration velocity analysis of 2D P-wave data from TTI media

Ernesto V. Oropeza[1] and George A. McMechan[1]

ABSTRACT

We have developed a common-reflection-point (CRP)-based kinematic migration velocity analysis for 2D P-wave reflection data to estimate the four transversely isotropic (TI) parameters V_{P_o}, δ, and ε, and the tilt angle ϕ of the symmetry axis in a TI medium. In each iteration, the tomographic parameter was updated alternately with prestack anisotropic ray-based migration. Iterations initially used layer stripping to reduce the number of degrees of freedom; after convergence was reached, a couple of more iterations over all parameters and all CRPs ensured global interlayer coupling and parameter interaction. The TI symmetry axis orientation was constrained to be locally perpendicular to the reflectors. The V_{P_o} dominated the inversion, and so it was weighted less than δ and ε in the parameter updates. Estimates of δ and ε were influenced if the error in ϕ was $>5°$; estimates of V_{P_o} were also influenced if the error in ϕ was $>10°$. Examples included data for a simple model with a homogeneous TI layer whose dips allowed recovery of all anisotropy parameters from noise-free data, and a more realistic model (the BP tilted transversely isotropic (TTI) model) for which only V_{P_o}, δ, and ϕ were recoverable. The adequacy of the traveltimes predicted by the inverted anisotropic models was tested by comparing migrated images and common image gathers, with those produced using the known velocity models.

INTRODUCTION

Estimating anisotropy in complex media has long suffered from the inherent trade-off between the parameters that describe the anisotropic behavior of the wavefield. The resolution of this trade-off requires angular coverage that is typically beyond the recording aperture of conventional surface seismic acquisition. Approximate, but reliable and very efficient, algorithms that estimate anisotropic velocity models have value to provide overall initial views of the geometry of anisotropic structures, for input to improve imaging of anisotropic media, and as starting models to a more complete (e.g., full-wave) inversion. The implementation and testing of such an algorithm is the topic of this paper.

Developments in seismic imaging include algorithms for transversely isotropic (TI) media. Sena and Toksöz (1993) develop asymptotic expressions for TI Kirchhoff migration. Kumar et al. (2004) apply 2D Kirchhoff migration to P-waves in anisotropic media. Anderson et al. (1996) include a VTI parameterization in a phase-shift migration. Alkhalifah (1997) shows the improvements in a seismic image when using VTI migration instead of isotropic migration of real data. Ren et al. (2005) develop wave-equation migration for data from VTI media. Alkhalifah (1995) and Zhu et al. (2007) extend isotropic Gaussian-beam migration to TI media. Ferguson and Margrave (1998), Du et al. (2007), and Fletcher et al. (2009) develop a reverse-time migration (RTM) for tilted transversely isotropic (TTI) media. Dong and McMechan (1993) develop 3D RTM for P-waves. Oropeza and McMechan (2013) develop parsimonious prestack migration (Hua and McMechan, 2003) for TTI media. Although anisotropic migrations are available, obtaining an anisotropic velocity model for input to these migrations is still a current and challenging research topic (e.g., Wang and Tsvankin, 2013), motivating the approach in this paper.

Anisotropic migration requires an anisotropic velocity parameterization. Several authors have made efforts to obtain Thomsen's (1986) parameters (V_{P_o}, ε, and δ) from seismic P-wave data by migration velocity analysis (MVA). Sarkar and Tsvankin (2004) invert for ε, δ, and (vertical and horizontal) gradients of V_{P_o} for VTI media; V_{P_o} is assumed to be known at a central point in each layer, and velocity updates involve minimization of the residuals of the moveouts. Behera and Tsvankin (2009) use the same methodology for TTI media. Huang et al. (2007) invert for δ and ε with a joint tomographic inversion for areas where V_{P_o} can be accurately obtained at well locations with vertical check shots. Cai et al. (2009) and He

Manuscript received by the Editor 6 August 2013; revised manuscript received 18 December 2013; published online 2 May 2014.
[1]The University of Texas at Dallas, Center for Lithospheric Studies, Texas, USA. E-mail: oropezaev@utdallas.edu; mcmec@utdallas.edu.

and Cai (2011) use migration focusing analysis for VTI and TTI media; they build a VTI model from an initial isotropic model and then calculate the anisotropy axis orientation from the VTI image and update the TTI model for ε and δ. Kumar et al. (2008) do depth-migration analysis for a TTI model by comparing common focus point operators. They invert for ε and δ and iteratively estimate the orientation of the symmetry axis assuming that it is locally orthogonal to each layer bottom. Wang and Tsvankin (2013) update TTI parameters by a 2D gridded ray-based tomography that includes walkaway VSP traveltime residual data in the objective function.

The reflection traveltimes in TTI media vary with the orientation of the anisotropic symmetry axis ϕ (Tsvankin and Grechka, 2011). Jiang et al. (2009) demonstrate the influence of symmetry axis orientation in tomographic inversion of the anisotropic parameters. The ϕ represents an extra parameter (along with V_{Po}, ϵ and δ) to be recovered from moveout data (Tsvankin and Grechka, 2011). However, the inclusion and inversion of ϕ is not found in the MVA literature because it is nonunique and usually not considered to be solvable for surface data without geologic constraints (Tsvankin et al., 2010). Alkhalifah (2011) presents a solution for P-waves using perturbations from an elliptically anisotropic background. Below, the symmetry-axis orientation is estimated with a priori information such as geological setting (e.g., a dipping fracture system or progradational sequences [Dewangan and Tsvankin, 2006]). The axis of symmetry in MVA is commonly assumed to be orthogonal to the reflectors (Kumar et al., 2008; Behera and Tsvankin, 2009; Ferla and Cibin, 2009; Zhou et al., 2011).

All the above methods are tomographic MVAs that are computationally expensive and include postmigration residual picking between iterations (Zhou et al., 2011). Fei and McMechan (2006a, 2006b) develop an efficient CRP-based MVA for isotropic media. In their methodology, picking is done only once at the beginning, in one reference common-offset section; the reflection points are migrated using an efficient "parsimonious" migration (Hua and McMechan, 2003), and the velocity inversion is based on maximizing the stacking amplitudes in CRP gathers.

Seismic reflection tomography inversion is an ill-posed problem even for isotropic media. The main difficulties for anisotropic MVA are caused by the multiparameter nature of the problem and the trade-off between the model parameters (Tsvankin and Grechka, 2011). For 3D TTI media, five parameters have to be included and inverted: V_{Po}, ε, δ, and the orientation of the anisotropic axis (tilt and azimuth). The azimuth is constrained when inverting 2D data. This problem is reduced to an inversion for V_{Po}, ε, and δ when the anisotropic axis is constrained, but it still does not produce a unique solution. Various simplifications have been attempted, including TTI tomography by constraining ε and δ and updating only V_{Po} (Charles et al., 2008; Huang et al., 2008). Zhou et al. (2011) estimate V_{Po}, ε, and δ simultaneously; they show that multiparameter inversion provides a better data fit than V_{Po} only inversion but does not eliminate trade-offs between the TTI parameters when using only P-wave reflections. Other inversions constrain the anisotropy parameters by including well data (Bakulin et al., 2009; Ferla and Cibin, 2009). However, in frontier areas, well data are sparse or may not be available.

In this paper, we extend the isotropic 2D CRP-based MVA of Fei and McMechan (2006a) for P-wave reflection data from TTI models. The algorithm is ray-based and the anisotropy parameter values are estimated at each iteration in four main steps: (1) A prestack ray-based migration defines reflection points and the orientations of the reflectors at the CRPs. (2) Rays traced upward from each CRP define the data traces in the corresponding CRP gather. (3) Local updates are determined within each CRP by perturbations of each parameter to find the combination that maximizes the stack amplitude along the corresponding traveltime trajectory. (4) Finally, a global update is performed for each parameter at each grid point using the average values over all the locally predicted values from the CRPs that sample that point, and so it is a tomographic formulation. Iterations are first done for each initial layer in turn, from the surface downward; this layer stripping reduces the number of parameters to be solved at each iteration. After all parameters are converged for all layers individually, the resulting model is used as the starting model for two more iterations over all CRPs to reintroduce inter-CRP coupling.

The parameterization of the inversion consists of Thomsen's (1986) parameters (V_{Po}, ε, and δ) and the tilt angle of the symmetry axis ϕ; we invert for perturbations (ΔV_{Po}, $\Delta\varepsilon$, and $\Delta\delta$) instead of velocity ratios as in the isotropic CRP analysis (Fei and McMechan, 2006a, 2006b). This inversion does not inherently overcome the ill-posed problem of estimating Thomsen's parameters from surface seismic data, but it is effective when including constraints as proposed by the authors above. The methodology is purely kinematic and is ideal to perform TTI MVA because no picking of residuals is needed and the symmetry axis orientation is determined implicitly from the migration by setting it to be orthogonal to the local reflector orientation. We use anisotropic parsimonious prestack depth migration (Oropeza and McMechan, 2013) to obtain the position and orientation of the reflection points. We reduce the weight of the best-fit solution of V_{Po} and invert for $\Delta\varepsilon$ and $\Delta\delta$ simultaneously. Layer stripping is applied to invert for the anisotropic parameters from groups of CRPs that are interpreted to correspond to reflectors. This methodology is tested below with two TTI models: A homogeneous one-layer over a half-space model with a tilted symmetry axis, to illustrate the procedure, and a portion of the BP TTI model (http://www.freeusp.org/2007_BP_Ani_Vel_Benchmark/listing.html) to show the performance in a more realistic case. The parsimonious anisotropic migration (Oropeza and McMechan, 2013) is performed to locate CRPs and for quality control during the inversion.

EXTENSION OF CRP VELOCITY ANALYSIS TO 2D TTI MEDIA

The methodology for anisotropic CRP MVA uses the same framework as for the isotropic (Fei and McMechan, 2006a, 2006b), which consists of an iterative sequence of three steps: (1) prestack migration, (2) CRP gather building and local parameter estimation, and (3) global anisotropy updates. Modifications of the isotropic CRP MVA are required for application to data from TTI media. Figure 1 shows the flowchart for the TTI implementation. The following subsections describe each of the steps in detail.

Model parameterization and generation of test data

The parameterization of a 2D TTI medium includes Thomsen's (1986) parameters ε and δ as well as the P-wave phase velocity V_{Po} along the symmetry axis, and the tilt of the symmetry axis; ε and δ are dimensionless ratios. In 2D, the anisotropic symmetry axis orientation ϕ is measured in degrees in the range of -90 to $+90°$ from

the upward vertical direction, with positive angle measured clockwise. The Thomsen parameters γ and V_{So} are not necessary to the MVA because only P-waves are considered. However, those parameters are required input by the ray-tracing package ANRAY (Gajewski and Pšenčík, 1990) because its parameterization consists of the elastic tensor. Thus, we set $\gamma = \epsilon$ and $V_{So} = 0.5\,V_{Po}$ to be able to calculate the elastic tensor from the Thomsen parameters (Oropeza and McMechan, 2013). The parameters are specified over a rectangular grid mesh for heterogeneous models; so each grid box has four values (V_{Po}, ε, δ, and ϕ) associated with it.

Now, we illustrate the details of the anisotropic CRP MVA algorithm through a simple example that uses synthetic data for a model (Figure 2a) with a TTI layer over an isotropic half-space. The model grid has dimensions 1001×201 grid points, with a grid increment of 10 m in both directions. The simulated data for the TTI model have 101 sources separated by 50 m, extending from 1 to 6 km along the top of the model and 501 receivers at an interval of 10 m. All the receivers are off-end and located to the right of each source position. The anisotropic traveltimes for the synthetic survey are calculated by ray tracing by using ANRAY 4.7. The unit amplitude spike at each traveltime is convolved with a Ricker wavelet, with a dominant frequency of 60 Hz, to produce the synthetic data (e.g., Figure 3a).

Prestack anisotropic migration

Oropeza and McMechan (2013) describe the anisotropic parsimonious migration used in the CRP MVA. The reflection times are picked only once, from a few prominent control horizons in one reference common-offset section, and are used to build the CRP gathers at each iteration through the MVA. Each picked reflection traveltime corresponds to a source-receiver pair. Horizontal slowness (p-value) estimation is performed by local slant stacking (Hua and McMechan, 2003) for each reflection point, in the common-source gathers, corresponding to the reflections in the reference common-offset section. In this implementation, horizontal slownesses are calculated only at each receiver position because surveys are commonly insufficiently sampled in the source dimension to produce reliable p-values. The source-to-reflector portion of the raypaths are obtained by iterative two-point ray tracing to satisfy the image time condition.

The p-values are used to calculate the initial angle of the raypath from the receivers to perform the anisotropic parsimonious depth migration, only of the picked reference reflections (Oropeza and McMechan, 2013); the anisotropy is included in the ray tracing. However, the initial model for the inversion could be either anisotropic or isotropic. At each iteration, the reflection points are obtained by migration with the updated velocity model. The measured p-values do not change with the model, but the initial angles of rays at the receivers change with updates of the anisotropic velocity model at each iteration and so the positions and orientations of the migrated reflection points are also changed. We use only

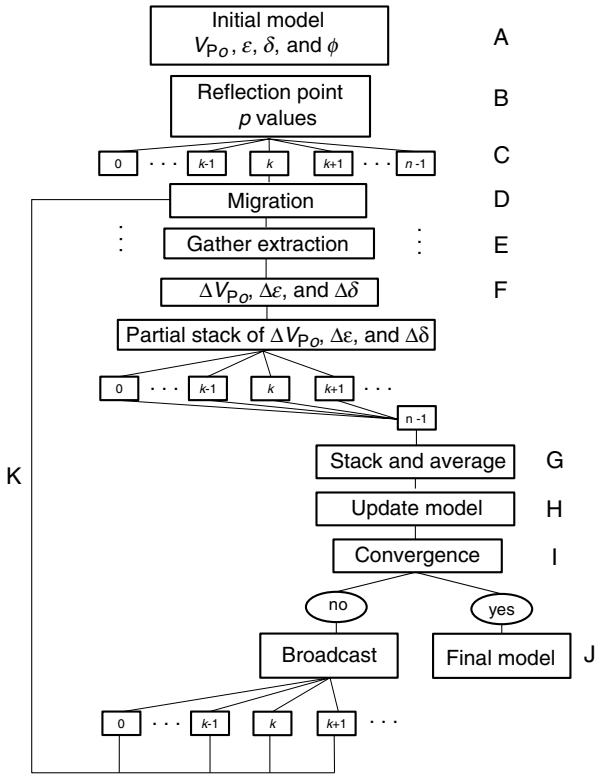

Figure 1. Message passing interface (MPI) flowchart for the anisotropic CRP MVA; n is the number of processors.

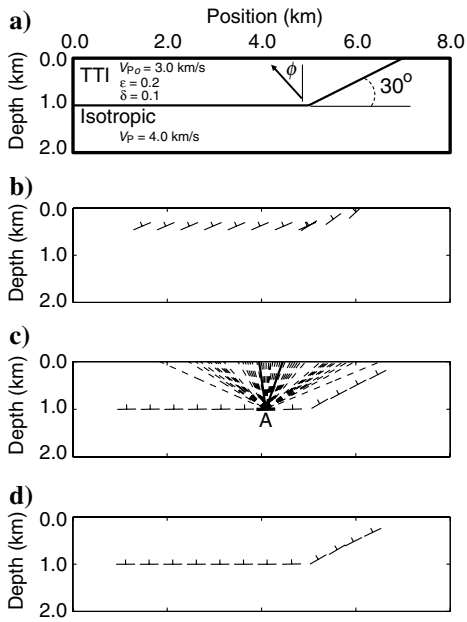

Figure 2. (a) TTI homogeneous layer model. The arrow in (a) indicates the orientation of the symmetry axis ϕ (−30°) that is orthogonal to the dipping interface in the model. The horizontal position of the first shot of the survey is 1 km and the last shot is at 6.0 km. (b) Twelve representative migrated CRPs and reflector orientations obtained from migration using the initial (isotropic) velocity model of V_{Po} (1.5 km/s), and neglecting the TTI symmetry, ε and δ. (c) Twelve representative migrated CRPs and reflector orientations after iteration seven (constraining the symmetry axis to the correct orientation) and (d), using the correct model. Each reflection point corresponds to a CRP gather. The reflection points are plotted at an interval of 500 m between their corresponding source/receiver mid points. The dashed lines in (c) are the pairs of raypaths used to extract traces for that CRP gather at the seventh iteration; the solid line is the raypaths for the reference offset, used to image the reflection point A.

the local position and the orientation of the migrated reflection points. There is no need to build common image gathers (CIGs) for the CRP MVA, so the amplitudes are not distributed to make migrated seismic images at the intermediate iterations. Figure 2b shows the location and the orientation of local reflectors of representative picked reflection points along the reflector for the initial model. The apparent reflector dips in Figure 2b are a consequence of the neglected tilted TI symmetry in the starting model. Figure 2c shows the migrated reflection points after iteration seven; compare with the migrated reflection points obtained using the correct model (Figure 2d).

CRP gather building

The CRP gather at each reflection point is built by finding the traces, across common-source gathers, that contain the reflections that migrate to the CRP (Fei and McMechan, 2006a, 2006b). At each iteration, each CRP has a different CRP trace gather. Four calculations are involved in CRP gather building: migration of a reference-offset reflection with the current anisotropic velocity model to define the reflection point position and the orientation of the reflector (Figure 2), calculation of the incident/reflected angle at the reflection points, initial-value ray tracing of source and receiver rays from the reflection points to the surface, and selecting the data (seismic traces) with the source and receiver locations that are closest to the termination points of both raypaths at the surface. This avoids searching for raypaths that emerge at the source and receiver locations; tracing single rays is very efficient. The first three of these calculations are different for isotropic and anisotropic MVA. Another option to build the CRP gather consists of performing a two-point ray tracing from the reflection points to the sources and then tracing initial-value raypaths (that satisfy Snell's law at the reflector), to the surface to define the corresponding receiver position. However, this approach is less efficient because the two-point ray tracing takes longer than tracing a single initial-value ray.

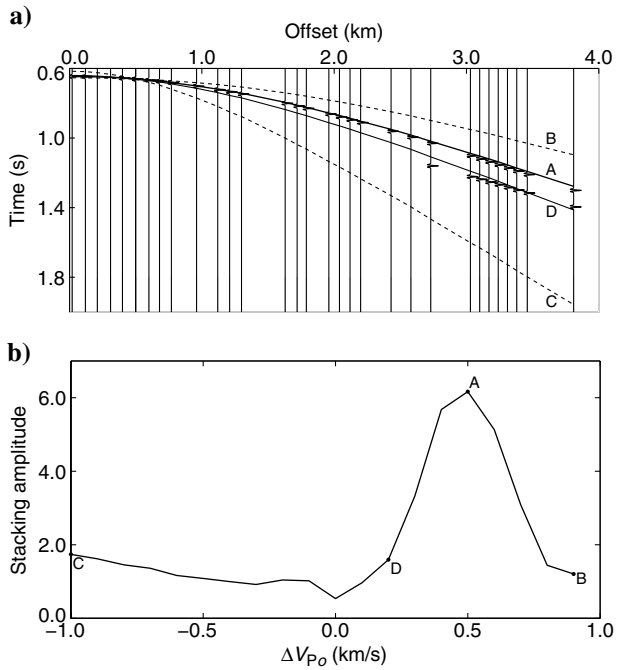

Figure 3. The V_{P_o} inversion at the fourth iteration. Panel (a) is a representative CRP gather for a reflection point. Traces are irregularly distributed because some incident-reflected raypaths did not arrive at the surface sufficiently close to source-receiver locations of the traces recorded for this CRP, and so are omitted. The range of ΔV_{P_o} is -1.0 to 0.9 km/s scanned at an increment of 0.1 km/s. Panel (b) shows the stacked amplitudes on the traveltime trajectories in panel (a). Labels C and B indicate the traveltime trajectories (in panel [a]) and stacking amplitudes (in panel [b]) for ΔV_{P_o} of -1.0 km/s and 0.9 km/s, respectively. In panel (b), A is the largest stacking amplitude and is obtained for ΔV_{P_o} of 0.5 km/s. Label D is the traveltime trajectory (in [a]) and the stacking amplitude (0.2 in panel [b]) after the damping factor (0.4) is applied.

Calculation of incident and reflected angles

Calculating the initial angles for an incident/reflected pair of raypaths at a CRP point is different for the isotropic and the anisotropic implementation. The take-off angles at the reflector need to satisfy Snell's law at the reflection point. In an isotropic medium, the incident and reflected angles of the rays at a reflection point are equal. In an anisotropic (TI) medium, the reflected and incident raypaths are symmetric only when the orientation of the anisotropic symmetry axis coincides with the orientation of the local normal to the reflector (Alkhalifah and Sava, 2010). We set the incident slowness vector and calculate its corresponding reflection slowness vector at the opposite side of the normal to the reflector. Snell's law states that the projections of the incident and reflected phase (velocity or slowness) vectors to the plane tangent to the reflector have to be equal (Dellinger, 1991; Tsvankin, 2005; Vavryčuk, 2006) (see Figure 2 in Oropeza and McMechan, 2013). We set the incident phase angle θ_s and then iterate on the reflected phase angle θ_r until the magnitude of the vector projections to the reflector is equal. An alternative faster, but approximate, calculation is given by Farra and Pšenčík (2013). We use the Newton method to speed convergence. Once the initial and reflected angles are calculated, the corresponding pairs of rays are traced upward from the reflection point (Figure 2c).

The above procedure is applied in the TTI CRP MVA even when the orientation of the symmetry axis is constrained to be orthogonal to the reflector, for two reasons. First, updates of the orientation of the symmetry axis are done after each iteration (see the anisotropy parameter inversion section below); so, when the gather building is done, the orientation of the anisotropic symmetry axis (calculated locally in the migration) has not yet been updated. Second, the updates of the orientation of the anisotropic symmetry axis are averaged with those of the neighboring CRPs; so, the orientation of the symmetry axis at a CRP is not (necessarily) the same as the orientation produced by the migration; they approach the same value as the inversion of the anisotropy parameters converges.

Initial-value ray tracing

Initial-value ray tracing upward from the reflection point is performed by solving the ray-tracing equations for laterally inhomogeneous, anisotropic, media given by Gajewski and Pšenčík (1987) as

$$\frac{dx_i}{dt} = A_{ijkl} p_l g_j g_k \tag{1}$$

and

$$\frac{dp_i}{dt} = -\frac{1}{2}\frac{dA_{mjkl}}{dx_i} p_m p_j g_k g_l, \tag{2}$$

where i, m, j, k, and l are the spatial coordinates indices (1, 2, and 3), $\mathbf{x} = (x_1, x_2, x_3)$ is the spatial position vector, t is the traveltime, $A_{ijkl} = C_{ijkl}/\rho$ is the fourth-rank elastic tensor C_{ijkl} normalized by the density, $\mathbf{p} = (p_1, p_2, p_3)$ is the slowness vector, and $\mathbf{g} = (g_1, g_2, g_3)$ are unit polarization vectors. The symbols $v_j = d\mathbf{x}_i/dt$ are components of the group velocity vector.

Selection of CRP traces

Source-receiver pairs are defined by the ends of the raypath pairs from the CRP where they arrive at the recording surface. The ends of the raypaths do not exactly hit a receiver or source position; a maximum allowable distance error is set as a parameter so there is trade-off between efficiency and accuracy. The range of take-off angles from the reflection point is also set as a parameter. If angle increments are reduced, the chances to reach an acceptable match to a source or receiver position will increase, at the expense of computational time. The corresponding seismic trace for each source-receiver pair is copied to the CRP gather. Each reflection point has an associated area of the model that is sampled by all the pairs of raypaths traced from that reflection point. Figure 2c shows the rays calculated for the reflection point A at iteration seven.

At each iteration, a predicted (x, t) traveltime trajectory (Figure 3a) is produced for each CRP by ray tracing through the current model, from the CRP (e.g., labeled A in Figure 2c). This predicted time curve coincides with the maximum amplitude trajectory of the reflection in the CRP gather when the input velocity model is correct. At all iterations, and for all (anisotropy) parameter perturbations at one iteration, each time trajectory is constrained to coincide with the reflection data only at the reference offset (0.5 km in Figure 3) (Fei and McMechan, 2006a, 2006b). The CRP gathers, and the predicted traveltime curves, are inputs for the parameter inversion.

Inversion for anisotropy parameters

In the isotropic CRP analysis (Fei and McMechan, 2006a, 2006b), a family of predicted traveltime curves are calculated by perturbing the velocity model by multiplying it by a series of constant velocity ratios. The variation of the traveltime with velocity perturbations is linear. This allows the traveltime for each perturbed model to be calculated without retracing the rays. The best-fit new velocity model is the one for which the stacking amplitude along each time trajectory is maximum (A in Figure 3a). In contrast to the isotropic case, for anisotropy parameter estimation, the rays need to be retraced using the new anisotropy parameters to get the new traveltime predictions. If the anisotropic parameters are restricted to vary in specific ways (e.g., in factorized media Červený, 2001), then analytic solutions exist.

The inversion for Thomsen's parameters (V_{Po}, ε, and δ) are based on the prediction of the traveltime curve for the CRP gathers when V_{Po}, ε, and δ are perturbed individually, in turn in each iteration; the stacking amplitudes along the predicted traveltimes, through the CRP gather, are calculated for different combinations of parameter perturbations.

The model fitting is implemented by maximizing the stacked amplitude along the predicted (x, t) trajectory, so reflection times are only implicitly fitted. Thus, picking of the traveltime in the observed (x, t) data is not required because times are not constrained (except at the reference offset). The trace at the reference offset is always included in the CRP gather and its updated traveltime always coincides with the observed traveltime (Figure 3a) because it was picked from the reference common-offset gather. The reference traveltime must remain unperturbed, so the location of the reflection points have to be adjusted (Appendix A) at each iteration to satisfy this time condition. The goal of this inversion is to find the combination of V_{Po}, ε, and δ that produces the largest stacking amplitude at each reflection point.

Sensitivity of group velocity to changes in anisotropy

In an isotropic medium, if the velocity is everywhere perturbed by a constant factor α, the raypaths do not change, and the fractional change in the traveltime is the same as the fractional change in velocity (Fei and McMechan, 2006a). For anisotropic media, the traveltime perturbation depends on the anisotropic axis orientation and Thomsen's parameters, so the traveltime steps along the raypaths need to be kept. The contribution of a representative raypath segment d to the total traveltime perturbation is given by

$$\Delta T = -\frac{d}{v_g^2(\psi)}\Delta v_g, \tag{3}$$

where ΔT is the time change in a step distance d along the raypath, $v_g(\psi)$ is the group velocity along the ray segment before the velocity perturbation for the angle ψ with the anisotropic axis and

$$\Delta v_g = \frac{\partial v_g}{\partial V_{Po}}\Delta V_{Po} + \frac{\partial v_g}{\partial \varepsilon}\Delta\varepsilon + \frac{\partial v_g}{\partial \delta}\Delta\delta. \tag{4}$$

In equation 4, the partial derivatives with respect to V_{Po}, ε, and δ are assumed to be locally constant in the ray-step increment d. Figure 4a and 4c shows the variation of v_g with V_{Po}, ε, and δ for propagation angles of 0° (along the symmetry axis), and 30°, 60°, and 90° from the symmetry axis, for the anisotropy parameters defined in the caption to Figure 4, calculated by (Postma, 1955; Dellinger, 1991; Carcione, 2007):

$$v_g = \sqrt{v_P^2 + \left(\frac{dv_P}{d\psi}\right)^2}, \tag{5}$$

where the phase velocity (v_P) is calculated by Thomsen (1986) as

$$v_p^2(\psi) = {V_{Po}}^2[1 + \varepsilon\sin^2\psi + D(\psi)], \tag{6}$$

with $D(\psi)$ is given by

$$D = \frac{1 - {V_{So}}^2/{V_{Po}}^2}{2}\left[\left[1 + \frac{4(2\delta - \varepsilon)}{(1 - {V_{So}}^2/{V_{Po}}^2)}\sin^2\psi\cos^2\psi + \frac{4(1 - {V_{So}}^2/{V_{Po}}^2 + \varepsilon)\varepsilon}{(1 - {V_{So}}^2/{V_{Po}}^2)^2}\sin^4\psi\right]^{1/2} - 1\right]. \tag{7}$$

The variation of v_g with V_{Po} is linear for all V_{Po}. The variation of v_g with ε (Figure 4b) is nearly linear and fairly flat in the range shown, so the traveltime perturbation for variation of ε will be small for each iteration. Figure 4c shows the variation of v_g with δ; it is also linear, with derivatives close to zero at all propagation angles. Figure 4d shows the variation of v_g with the orientation of the symmetry axis ϕ when V_{Po}, ϵ, and δ are constant; unlike the variation of the other anisotropy parameters, $\partial v_g/\partial\phi$ is nonlinear and so would need to be calculated at each iteration for each time step of the raypath if it were included in the inversion. If the anisotropic axis orientation is known or calculated from the migration (e.g., orthogonal to the orientation of the local reflector), then the calculation of the partial derivatives of v_g is done numerically, and once, for the whole perturbation range of V_{Po}, ε, and δ. Equivalent simpler expressions for traveltime perturbations under specific conditions of dip-constrained weak anisotropy are given by Farra and Pšenčík (2013), and for smooth anisotropic media, by Červený (2001).

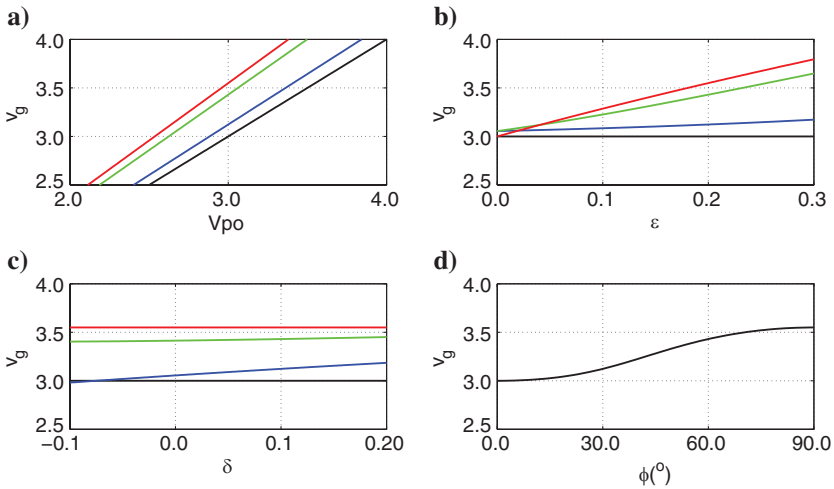

Figure 4. Group velocity as function of (a) V_{Po}, (b) ε, (c) δ, and (d) the axis of symmetry orientation ϕ. The V_{Po} is 3 km/s in (b-d). The ε is 0.2 in (a, c, and d). The δ is 0.1 in (a-d). The black lines in (a-c) are for the propagation at 0° (along the axis of symmetry). The blue lines in (a-c) correspond to a propagation angle of 30°; the green lines to 60° and the red lines to 90° (orthogonal to the axis of symmetry).

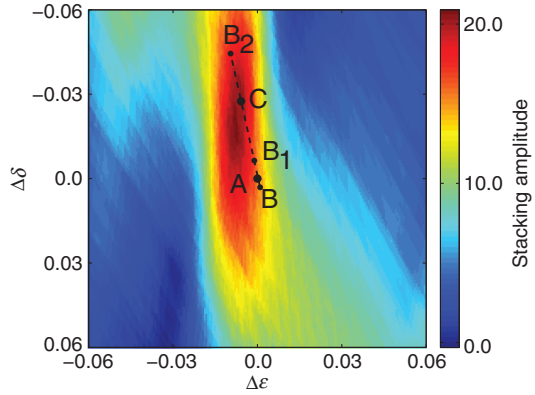

Figure 5. Steepest descent on the ($\Delta\varepsilon$, $\Delta\delta$) plane applied at the fourth iteration (see Figure 3 for the prior ΔV_{Po} calculation at this iteration). A to C are the steps to estimate the location of the maximum stacking amplitude. The gradients are locally calculated at A and B. B, B_1, and B_2 are used to calculate C. C defines the perturbations $\Delta\varepsilon$ and $\Delta\delta$ to be applied at the current iteration. See also Figure 6.

Inversion strategy

Each combination of ΔV_{Po}, $\Delta\varepsilon$, and $\Delta\delta$ (within the ranges selected for the inversion) produces a time trajectory, and a stacking amplitude along that trajectory. The goal is to approach to the correct parameter values iteratively. To estimate ΔV_{Po} at each iteration, ε, and δ are fixed at their values at the previous iteration, and the stacking amplitude is calculated for the allowed range of ΔV_{Po}. The V_{Po} update value (ΔV_{Po}) that corresponds to the highest stacking amplitude is not applied directly; a smaller update is used to reduce the dominant influence of V_{Po} on the solution. This reduced weighting (damping) of the V_{Po} updates makes V_{Po} converge more slowly, but it allows δ and ε to contribute. This is similar to damping of a least-squares solution to facilitate a balance between resolution and covariance (Menke, 1984).

Figure 3a shows the traveltime corresponding to the estimated V_{Po} at the fourth iteration. The dashed lines are the perturbed traveltimes for ΔV_{Po} of −1.0 km/s (for curve C) and 0.9 km/s (for curve B) while ε and δ are fixed (at ∼0.066 and ∼0.076, respectively). Figure 3b shows the stacking amplitudes for each perturbed traveltime curve. The largest stacking amplitude corresponds to ΔV_{Po} of 0.5 km/s at this iteration. The damping factor used is 0.4; thus, the ΔV_{Po} applied at each iteration is 40% of the predicted update. Because the V_{Po} perturbations tend to zero as the solution converges, the effect of the damping factor is minimized in the final solution (40% of zero is still zero).

Evaluating how far V_{Po} is from the correct solution is straightforward because it has the major influence on the traveltime trajectory (Figure 3a) (Thomsen, 1986). To have a well-conditioned inversion, the elements of the sensitivity matrix should (ideally) have similar orders of magnitude (so each model parameter is weighted similarly). Figure 4 shows that the sensitivity of v_g (and hence of the traveltime) to V_{Po} is larger than to ε and δ. The damping factor applied to ΔV_{Po} is an approximate compensation.

The estimated perturbation (ΔV_{Po}) of V_{Po} is then fixed to calculate $\Delta\varepsilon$ and $\Delta\delta$ (via equations 3 and 4). To avoid comparing stacking amplitudes for all the possible values of $\Delta\varepsilon$ and $\Delta\delta$, a numerical approach is applied to locate the maximum stacking amplitude in the ($\Delta\varepsilon$, $\Delta\delta$) plane. Because there is no analytic expression for the ($\Delta\varepsilon$, $\Delta\delta$) surface, we apply the approximation of Shewchuk (1994); a parabola is fitted through three points along the direction of the largest local amplitude gradient at each step (Figure 5). The gradients might not point to the absolute maximum in intermediate iterations, as they are calculated locally. Figure 6 shows the amplitudes along the segment B − B_2 on Figure 5 that is the second step in the steepest descent method when the current point is at B. The parabola fitted through the points labeled B, B_1, and B_2 reaches its maximum at C, which is an approximation to the largest stacking amplitude at C′, and defines the starting point for another step. The process stops when the amplitude gradient is nearly zero in all

directions at one point of the surface (indicating a maximum of the surface). Thus, the computational time is significantly reduced because there is no need to evaluate the points along the profile direction in a shorter interval to obtain the actual stacking amplitude maximum. The ΔV_{P_o}, $\Delta\varepsilon$, and $\Delta\delta$ tend to zero as the procedure continues and approaches the solution.

Results from the homogeneous layer example

To complete the homogeneous anisotropic layer example used in the previous subsections consider the results as iterations proceed. Because the layer is homogeneous, only single values of V_{P_o}, ε, and δ are solved for. The initial V_{P_o} is 1.5 km/s everywhere, and the initial ε and δ are zero (an isotropic medium). Figure 7a–7c shows the values of V_{P_o}, ε, and δ during 20 iterations. The horizontal dashed lines are the correct values of each parameter ($V_{P_o} =$ 3.0 km/s, $\varepsilon = 0.2$ and $\delta = 0.1$). Figure 7d shows the rms change in the traveltime caused by the updates of V_{P_o}, ε, and δ at each iteration. Convergence of the model is indicated by the concurrent flattening of the parameter trajectories (Figure 7a–7c) to the correct values and of the traveltime update trend (Figure 7d) to a stable minimum (ideally zero).

With the values of ΔV_{P_o}, $\Delta\varepsilon$, and $\Delta\delta$ for each CRP as input at each iteration, the model is updated. Because the medium is constrained to consist of homogeneous layers, the updates are averaged and all the grid points in the considered layer are assigned the same updated value. Another iteration starts if the rms difference of the traveltime has not reached stable minimum values (Figure 7d).

All three anisotropy factors are recovered because flat and dipping segments of the reflector (Figure 2a) together provide a wide propagation angle aperture. In this example, the symmetry axis orientation (not shown in Figure 7) was constrained to be normal to the dipping part of the reflector, at all iterations.

Inversion of heterogeneous media with virtual-layer stripping

For inversion of a homogeneous medium, it is assumed that V_{P_o}, ε, and δ are constant in each of the pseudolayers defined by the selection of the marker reflections in the reference-offset section. For heterogeneous media, V_{P_o}, ε, and δ vary within the rectangular grid mesh, and the anisotropic parameter updates in each grid box are obtained by averaging the updates over all the CRPs that sample that grid box (Fei and McMechan, 2006a, 2006b). Because the model is unevenly sampled, interpolation and smoothing are applied to stabilize the solution. A threshold minimum number of samples (here 10) is required to be met for the parameters in a grid box to be updated; tests by Crosson (1976) indicate a minimum of 10 for field data. Parameter updates for grid points that are not sampled, or are sampled by fewer than the threshold number, are obtained by interpolation (or extrapolation). Smoothing (by averaging the values in square overlapping areas centered on each grid box) is performed to avoid sharp edges that may affect the ray tracing in the next iteration. In the CRP gather building, the incident and reflected angles need to be calculated even when the symmetry axis is constrained to be orthogonal to the reflector (e.g., the dipping part of the model in Figure 2a) because ϕ is averaged in each grid box from CRPs that sample that box.

A CRP group is defined as those CRP positions that are associated with a single reflector. When there is more than one group of CRPs, layer stripping is used (Fei and McMechan, 2006a, 2006b). The layer stripping consists of inverting the data for each virtual layer in turn, from shallowest to deepest. When inverting a

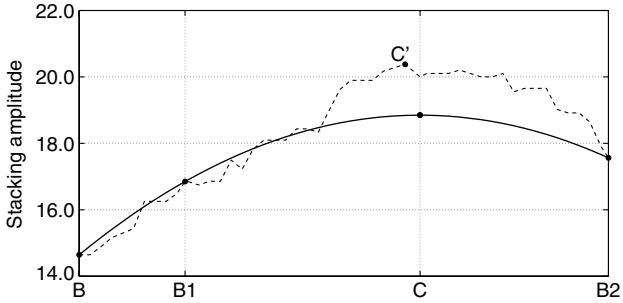

Figure 6. Calculation of the update for one step of the steepest descent method. The dashed line represents stacking amplitudes along profile $B - B_2$ in Figure 5. The solid line is a parabola calculated from the amplitudes at B, B_1, and B_2; the stacking amplitude is calculated only at these points. C is the output position in the ($\Delta\varepsilon$, $\Delta\delta$) plane for the current step. The C′ is the actual maximum amplitude in the profile $B - B_2$.

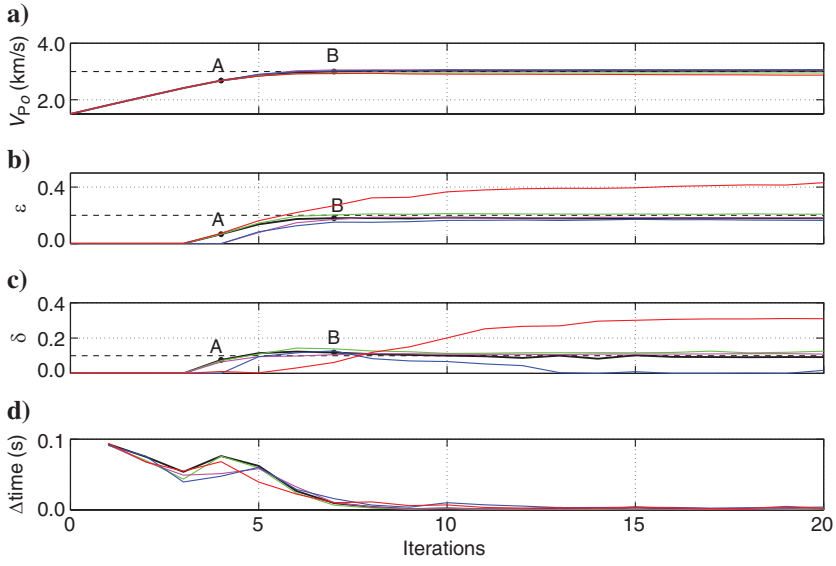

Figure 7. Twenty iterations of TTI model inversion. (a) is V_{P_o}, (b) is ε, (c) is δ, and (d) is the rms change in traveltime updates over all CRPs at each iteration. The black solid line corresponds to the inversion when the anisotropic axis orientation is constrained to be correct (−30°) (Figure 2). Label A is the estimated model at the fourth iteration (refer to Figures 3 and 5) and label B is for the estimated model at the seventh iteration (refer to Figure 2c). The green and purple lines correspond to the inversion with an error of 5° in the orientation of the anisotropic axis (−25° and −35°, respectively). The blue and red lines correspond to the inversion with an error of 10° in the orientation of the anisotropic axis (−20° and −40°, respectively). The horizontal dashed lines in (a-c) are the correct values of each parameter.

subsequent group, the part of the model sampled by the groups previously inverted is considered to be correct and so is not perturbed; perturbations of V_{P_o}, ε, and δ are set to zero in the shallower layers and there are no updates to the parameters of these "layers" when inverting for those of the next-deeper group. The convergence criterion for each group is to minimize the change in the rms traveltime updates between those of the previous iteration and those predicted from the updated model (by equation A-4), for the current iteration. The rms of the differences is calculated over all traces for all the reflection points of the current group. Iterations for each group of reflection points stop when the rms difference reaches a stable minimum. A maximum number of iterations can also be set. We do more iterations than are necessary to ensure convergence is achieved. Layer stripping is applied in the example in the next section.

Symmetry axis orientation

The symmetry axis orientation ϕ is the most difficult parameter to estimate from surface reflection seismic data; it is ill conditioned (Barbosa et al., 2008). Figure 4d shows the nonlinear variation of the group velocity v_g with ϕ (unlike the other anisotropic parameters, Figure 4a–4c); thus, in the CRP MVA, ϕ should be assumed or constrained (Zhou et al., 2011). Assuming an incorrect symmetry axis orientation will affect the inversion of the other anisotropic parameters. In Figure 7a–7c, we compare the inversion for V_{P_o}, ε, and δ when the correct symmetry axis orientation is used with the inversion of the same parameters for errors of ϕ of $\pm 5°$ and $\pm 10°$. The ϕ may be estimated from geological information (e.g., the orientation of fractures (or shales) from cores, logs, or the regional geologic stress) to constrain the anisotropic axis orientation.

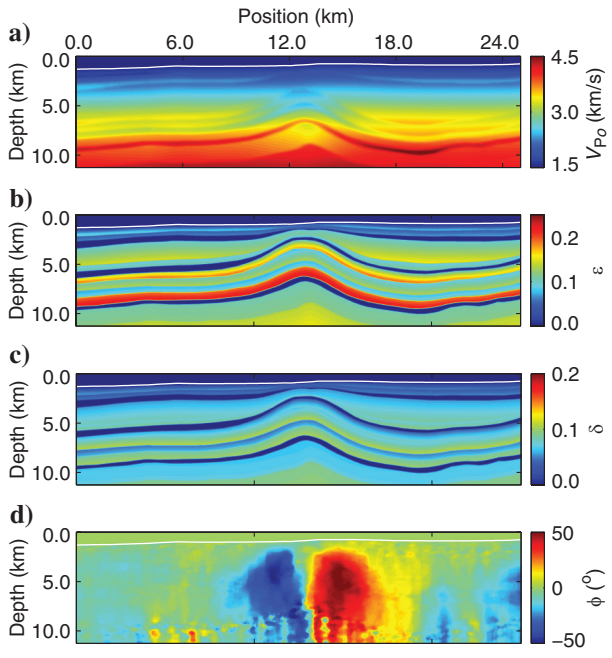

Figure 8. The BP TTI model. Panel (a) is V_{P_o}, panel (b) is ε, panel (c) is δ, and panel (d) is the anisotropic symmetry axis orientation ϕ (positive clockwise from vertical). The white line near 1-km depth in each panel is the water bottom.

If the anisotropy is assumed to be caused by alternation of higher and lower velocity layers (e.g., shales and sands), the axis orientation ϕ tends to be orthogonal to the bedding (Kumar et al., 2008; Behera and Tsvankin, 2009; Zhou et al., 2011). Thus, ϕ will change locally as the reflector shapes change from one migration to the next as a consequence of the velocity updates. When applying layer stripping, the model is updated after all the parameter perturbations; each grid point within the current layer is updated with the average updates determined for each of the CRPs that sample that grid point.

Numerical implementation

The CRP analysis is implemented in a parallel environment; we use the MPI. Figure 1 shows the flowchart. First (step A), the initial velocity model is loaded across the processors. The horizontal slowness of each reflection picked in the chosen reference common-offset section (step B) is input (step C) to parallel prestack parsimonious migration (step D); the location and orientation of the migrated reflection points are used as control points for CRP gather building (step E) and the parameter inversions (step F). The reflection points are organized into groups. Each processor does the CRP gather building and inversion of all reflection points in one or more groups. Reflection points that have less than a minimum number of usable traces are skipped; those reflection points may be used in subsequent iterations, as the velocity is updated.

The resultant ΔV_{P_o}, $\Delta\varepsilon$, and $\Delta\delta$ values and the traveltime update for each reflection point are sent from each processor to a master processor (step G), where averaging of the updates at each grid point is performed. The information on the area sampled by the raypaths (see the CRP gather building subsection) is also sent. The average of updates for each parameter is applied to the current model to produce the new model (step H) and the convergence criterion is checked (step I). If the convergence is achieved, (Figure 7) iterations stop (step J); if not, the master processor broadcasts the updated model to the other processors (step K) to start another iteration. When more than one group is present, a couple of final iterations are performed with all the CRPs together, using the result of the layer stripping as the starting model.

SYNTHETIC DATA EXAMPLE: BP TTI MODEL

Description of test data

As a more realistic example, anisotropic CRP analysis is applied to synthetic data for a portion of the 2D BP TTI model (Figure 8), which contains an anticline. The model is resampled from the original 6.25 m increment to 25 m in the x- and z-directions. The portion of the model used is 25 km horizontally and 11.2 km in depth. Figure 8a–8d shows the target V_{P_o}, ε, δ, and the orientation of the symmetry axis ϕ, respectively. The symmetry axes in this model are assumed to be locally orthogonal to the reflectors. The maximum water depth reaches 1294 m. The data we use for this example are calculated by finite differences and were downloaded from the website http://www.freeusp.org/2007_BP_Ani_Vel_Benchmark/listing.html. A time shift of 48 ms is applied to all traces so the maximum (zero phase) wavelet amplitude coincides with the reflection time (one period of the wavelet is ~96 ms).

We use 500 sources in a 25 km portion of the model with shot interval of 50 m and 800 receivers per shot with an interval of 12.5 m. All the receivers are off-end and located to the left of each

source position. The smallest offset is 37.5 m and the greatest offset is 10,025 m. The sources are at 6-m depth, and the receivers are at 8-m depth, in the water.

Data preprocessing

Five groups of reflection points are picked from the reference common-offset section (Figure 9). The red lines are the picked reference reflections. Each group has 501 reflection points that correspond to the number of traces of the reference common-offset section. A p (horizontal slowness) value is calculated for each picked reflection time.

The chosen reference offset (0.5 km) is short for the maximum offset (~10 km) in this survey. A reference section with a larger offset would be more sensitive to parameter changes, but the data quality is higher at shorter offsets and so are easy to pick, and thus, it is more appropriate to estimate the horizontal slownesses. The white line in Figure 8a–8d is the bottom of the water layer, for which the P-velocity is known and so remains unchanged during the MVA. In the CRP gather building, a maximum reflection angle of 40°, measured from the normal to the reflector, is set with an increment of 0.25°.

Inversion procedure and results

For the starting model for inversion, V_{P_o} is given (1.5 km/s) down to the water bottom, then a vertical gradient of 0.2 s^{-1} is added starting from the water bottom (based on the average increase of the velocity with depth). The other anisotropic parameters (ε and δ) are set to zero (i.e., assuming that the medium is isotropic). The tilt angle ϕ is orthogonal to the local reflection orientation; it is adjusted at each iteration after obtaining the new location and orientation of the CRPs.

CRPs that have migrated positions that are inconsistent with those of the adjacent CRPs are omitted from the velocity updates. These are usually a result of incorrect p estimations, or unreliable raypaths produced by high-velocity gradients, or they have too few rays (here 15) associated with them. The latter may still contribute at later iterations, as the velocity model improves. The incident and reflected angles are calculated at each CRP (even if the symmetry axis orientation is constrained to be orthogonal to the local reflector); ϕ is averaged at each grid point from CRPs that sample the respective grid points.

Layer stripping is applied sequentially through the CRP groups. Ten iterations are performed per group. The model is updated only in the region between the lines that separate the current and previous groups. After each iteration that updates all parameters at each grid point, the model is smoothed to avoid sharp edges between two consecutive regions. The model parameters and CRP positions change at each iteration as a result of the velocity model updates, and of the subsequent migration, respectively, at each iteration.

Figure 10a and 10b shows the CRP gathers for one point in group 2 at horizontal position ~7.5 km (Figure 9, second red line down from the top) at iterations one and 10. The red dashed lines are the traveltimes of the raypaths used to extract the traces in the CRP gather and the solid red lines are the traveltime updates by equation A-4, at the same iterations. In Figure 10b, these two traveltime trajectories overlie each other because the model above the CRPs of group 2 has converged. The damping used for V_{P_o} is 0.8 (see the parameter inversion section). Figure 10c is the same CRP gather shown in Figure 10b (the same source-receiver pairs and reference offset), also at ten iterations (during layer stripping) of group 2, with noise added.

After convergence is achieved for each group (or "virtual layer"), two additional iterations (without damping of V_{P_o}, or smoothing) are applied by allowing all the groups to vary simultaneously between the upper migration line (the water bottom in this case) and the line with the CRPs of the last inverted group in the layer stripping (Figure 11). Figure 12 shows the corresponding ray sample density.

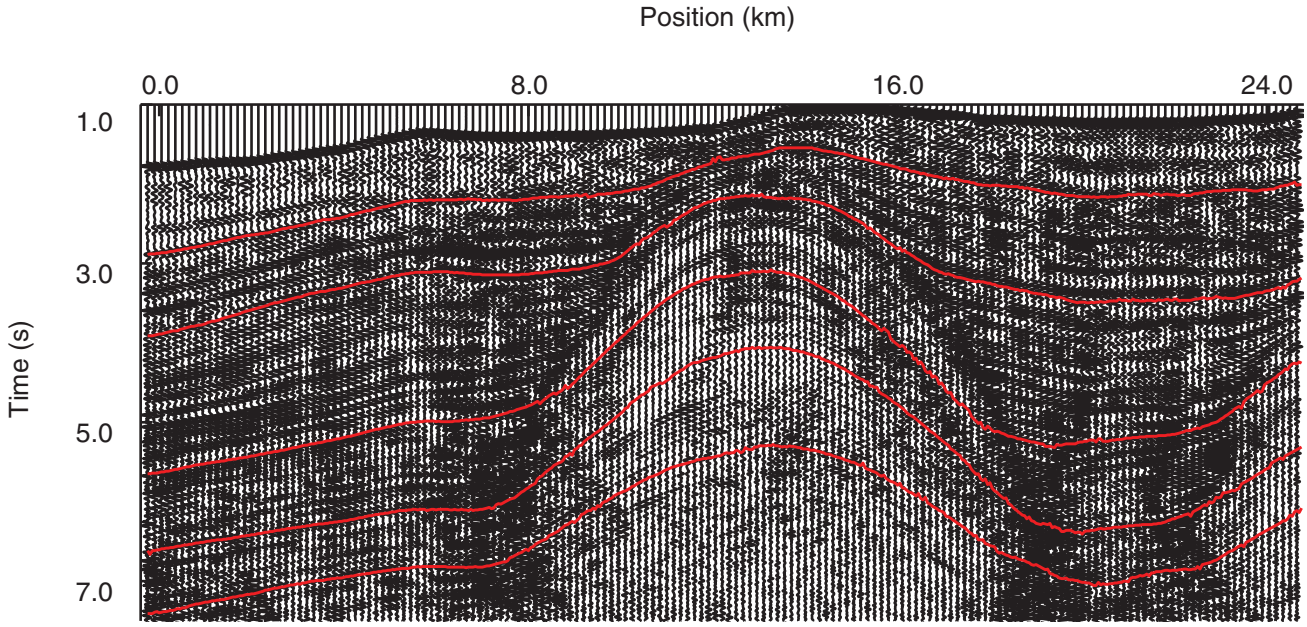

Figure 9. Reference common-offset (0.5 km) gather from the BP TTI data. The red lines are the picked traveltimes that are input to the CRP MVA. Each red line is a group: the top line is group 1, and the bottom line is group 5.

Figure 13a is the rms of the difference between the traveltime trajectories before and after maximizing the stack amplitudes in each of the five groups of CRPs by perturbation of V_{Po}, ε, and δ (equation A-4). Figure 13b–13d is the corresponding rms differences of the inverted perturbations of ΔV_{Po}, $\Delta\varepsilon$, and $\Delta\delta$, respectively, over the CRPs of each of the five CRP groups as a function of iteration number; rms differences are cumulative with increasing depth (increasing CRP group number). The final model is obtained by doing two additional simultaneous inversion iterations over the CRPs of all groups. The resulting rms differences for the two iterations are Δtime $\sim$32 ms (about 1/4 period), $\Delta V_{Po} = 0.05$ km/s, $\Delta\varepsilon = 0.003$, and $\Delta\delta = 0.002$ (see the two points at the right of Figure 13a–13d).

CIGs and stacked migrated section are calculated for quality control of the MVA. We use the parsimonious anisotropic migration (Oropeza and McMechan, 2013) for the prestack migrations. Figure 14a and 14b shows the migrated sections with the initial (isotropic) model and with the inverted model after iteration 12 (Figure 11), respectively. Figure 14c shows the migrated image obtained using a smoothed version of the correct model (Figure 8) that represents the best image that can be expected. Figure 15 shows the CIGs at 5, 13, and 18 km on the profile for the initial model, inverted model, and the correct (lightly smoothed) model. The final image (Figure 14b) is significantly different from that obtained with the starting model (Figure 14a) and is similar to the best expected solution (Figure 14c). Similarly, the CIGs for the final model (the center column in Figure 15) are flatter and very similar to those for the best solution (the right column in Figure 15) than to the CIGs for the starting model (the left column in Figure 15).

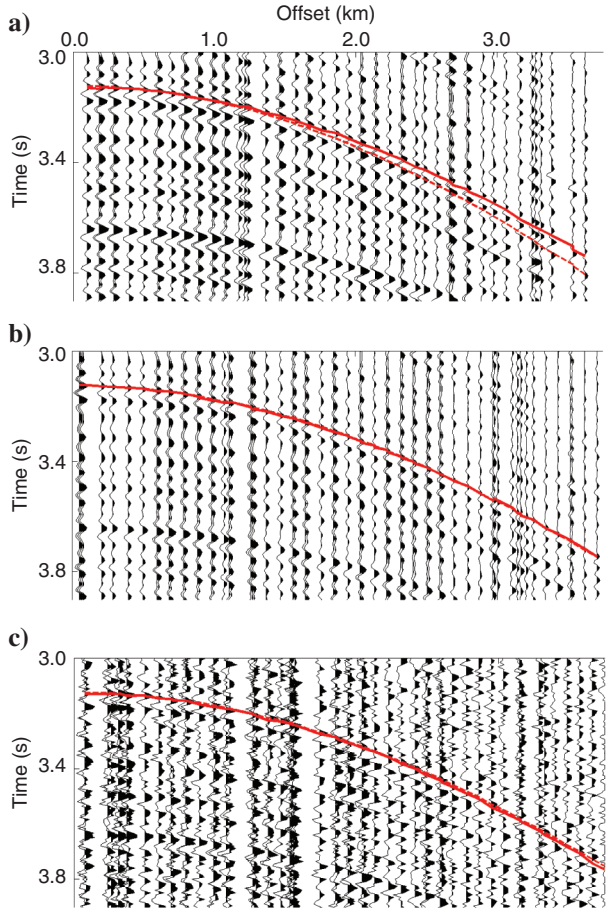

Figure 10. Representative CRP gathers of group 2 in Figure 9 at (a) iteration one, (b) iteration 10, and (c) iteration 10 when uncorrelated random noise is added. The dashed red line in each panel is the traveltime of the raypaths used to extract the traces in the CRP gather. The solid red line in each panel is the traveltime updated by equation A-4.

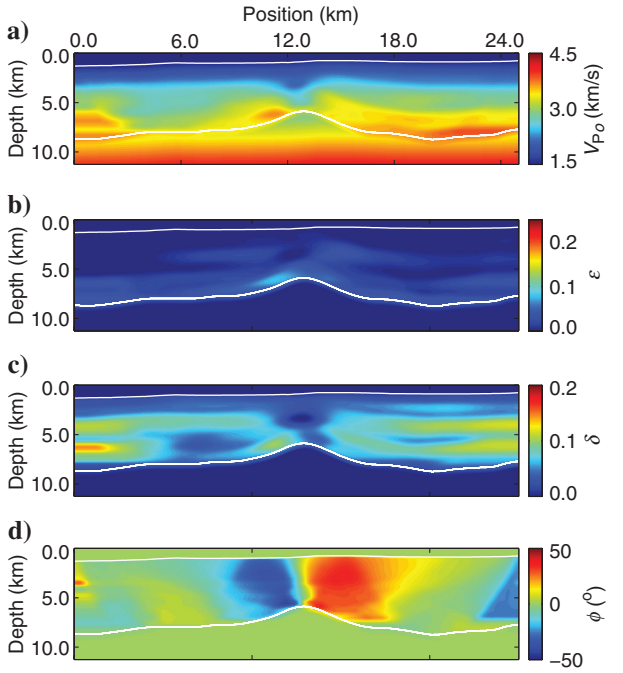

Figure 11. Final inverted velocity model obtained with all the CRP groups perturbed simultaneously for two iterations. The initial model is obtained by ten iterations per group of layer stripping. Panel (a) is V_{Po}, (b) is ε, (c) is δ, and (d) is the anisotropic symmetry axis orientation ϕ (positive clockwise). The damping factor for V_{Po} is 0.8. The top white line in each panel is the water bottom. The bottom white line is the locus of the migrated CRPs after iteration 10 of group 5 plus two simultaneous iterations of all parameters; values below this line are not sampled and so are not updated from the starting model in the inversion. Compare with the correct model in Figure 8. The artifacts near the edges are caused by low sampling and by CRPs with short offsets.

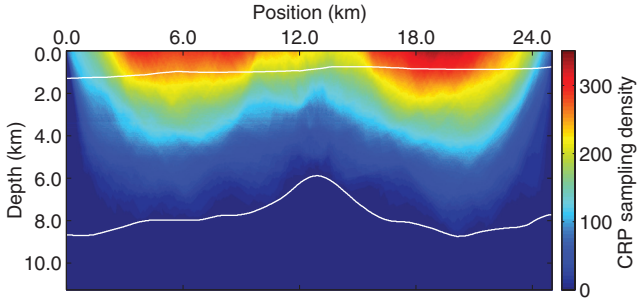

Figure 12. Sampling at grid points after iteration two of the simultaneous inversion of all groups (Figure 11) between the water bottom (the top white line) and the reflector position of group five (the lower white line).

DISCUSSION

The uniqueness of the traveltime trajectory that produces the largest (best fitting) stacked amplitudes on each CRP gather in the inversion (especially δ) is strongly affected by the frequency of the seismic data. For higher frequencies (smaller wavelengths), the change in stacking amplitude corresponding to small perturbations in traveltime is larger than for lower frequencies. Practical applications often estimate δ from well seismic data (Bakulin et al., 2009; Ferla and Cibin, 2009). The V_{P_o} may be found from check shots or well logs at borehole locations and used in combination with the stacking normal moveout (NMO) velocity to compute δ (Tsvankin et al., 2010).

The inversion for V_{P_o} and δ for the BP TTI model (Figure 11a and 11c) estimates a smoothed version of the corresponding correct values in Figure 8a and 8c. For V_{P_o} and δ, the quality of the inversion decreases with the depth of the CRPs used, as errors accumulate with increasing depth. The solution for ϵ is relatively poorly resolved (compare Figure 11b with Figure 8b) because ϵ is defined only by propagation angles that are far from the symmetry axes (Tsvankin, 2005) and the aperture in these data do not provide these constraints. Note the greater sensitivity of v_g to δ than to ϵ at angles <40° in Figure 4b and 4c.

Sampling density decreases with increasing depth (Figure 12), deeper regions are interpolated and smoothed to ensure consistency, but with the consequence of reduced resolution of the inversion. Sampling also decreases to the lateral edges of the model because of the survey geometry edges (off-end with receivers to the left); so these regions are also extrapolated and smoothed. The calculated ϕ at the right side of Figure 11d approximates the correct dips ϕ (Figure 8d); however, the shape of this region is affected by the extrapolation and low sampling.

The quality of the data also affects the inversion of the anisotropy parameters. In the simple synthetic traces (Figure 3a) from the homogeneous model (Figure 2a), all reflections have equal wave amplitude and the reflection moveout can be followed through most

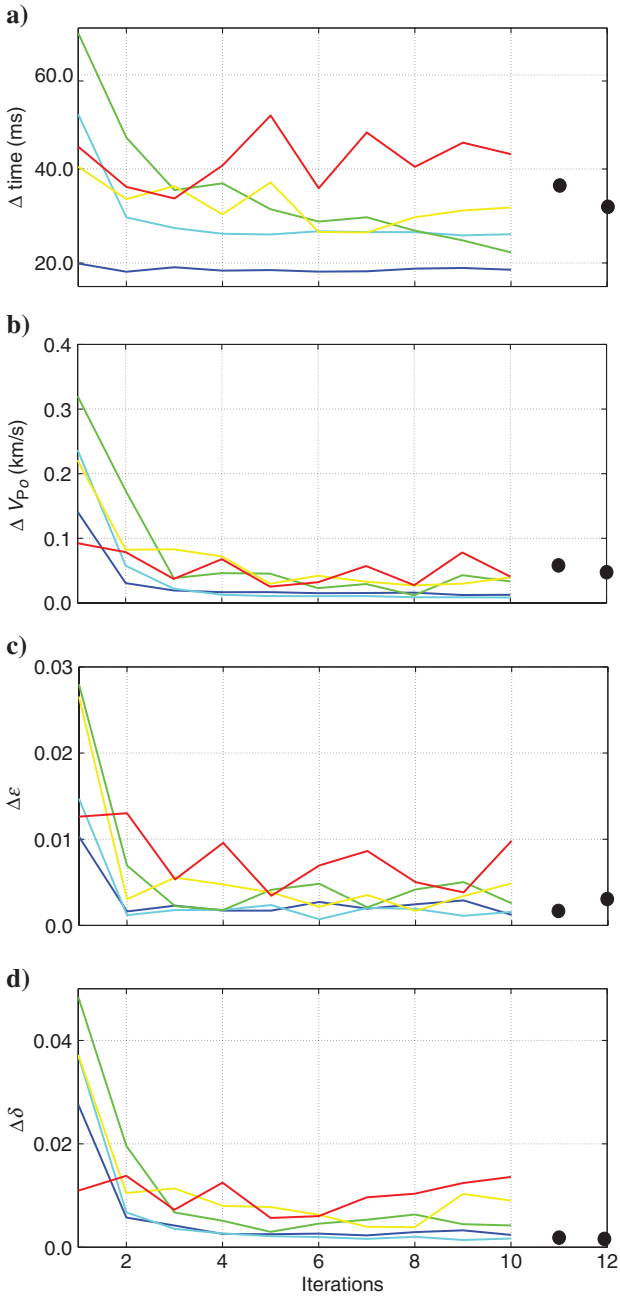

Figure 13. Rms updates per CRP within each CRP group for the inversion of the BP TTI data. Panel (a) is the rms change in traveltime updates over all CRPs at each iteration, panel (b) is for ΔV_{P_o}, panel (c) is for $\Delta\epsilon$, and panel (d) is for $\Delta\delta$. The dark blue, light blue, green, yellow, and red lines correspond to groups 1–5, respectively. The black dots at the right end of each plot are for two subsequent simultaneous inversion iterations of the CRPs of all groups; iteration 12 was accepted as the solution. The errors are cumulative with depth.

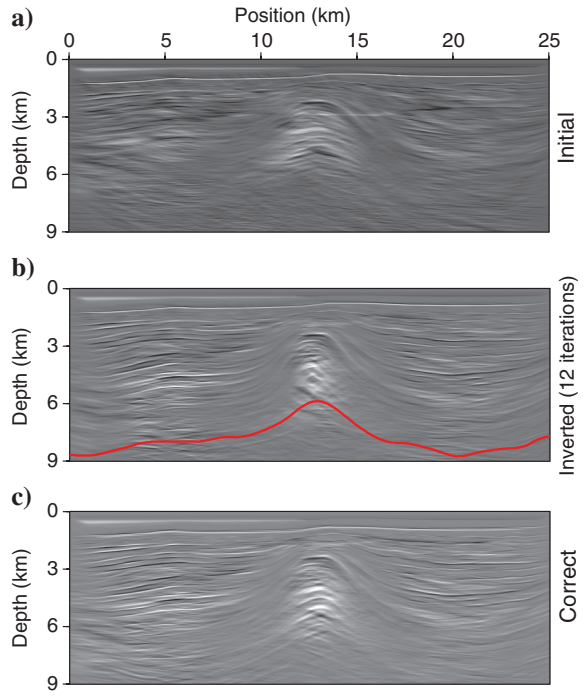

Figure 14. Migrated images of the BP TTI model using (a) the initial (isotropic) model, (b) the inverted model after ten iterations (of layer stripping) followed by two simultaneous iterations, and (c) a smooth version of the correct model. The red line in (b) shows the deepest group of reflection points used in the MVA.

of the offsets. The reflection moveouts in the finite-difference data of the BP TTI model are not visible in all the CRPs, or for all offsets (Figure 10c), even though they have strong reflections in the selected reference-offset section (Figure 9).

The rms of the model updates at each iteration (Figure 13a–13d) shows that the model converges for the two first CRP groups (the blue and light blue lines). For the deeper CRP groups (3, 4, and 5), the parameter updates are not smoothly decreasing as for the first two. Cumulative errors occur when applying layer stripping and affect the inversion of the deeper CRPs.

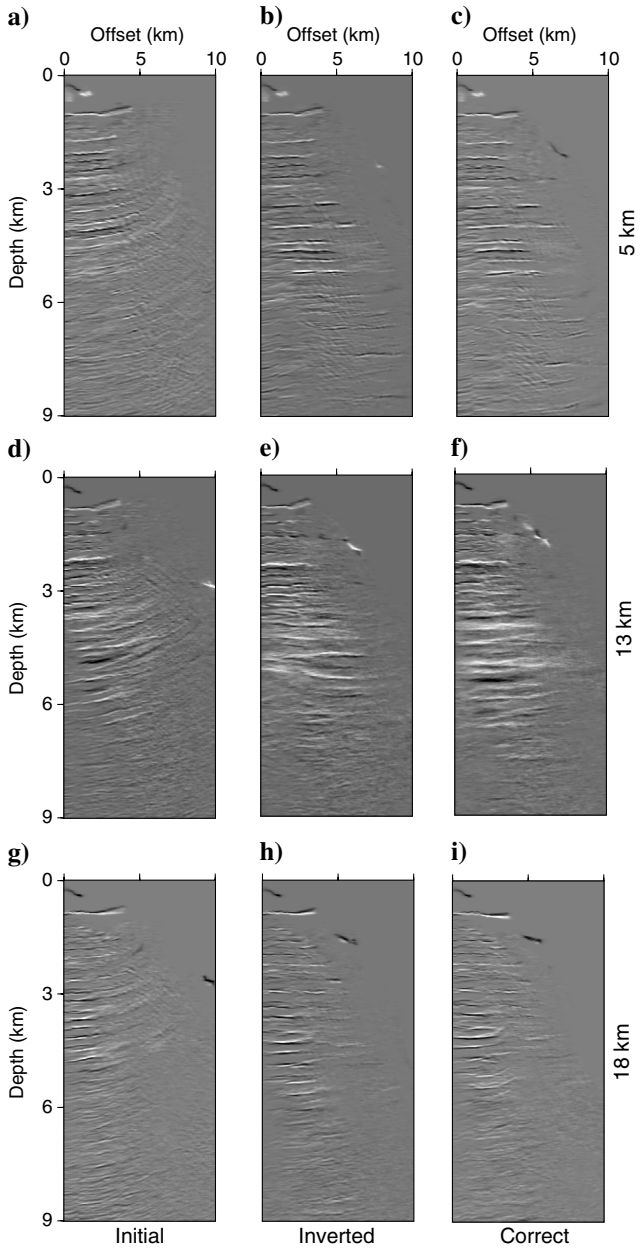

Figure 15. CIGs of the migration in Figure 14. Panels (a-c) are the CIGs for the initial, inverted (final model), and correct model, respectively, at 5 km on the profile. Panels (d-f) are the corresponding CIGs at 13 km on the profile. Panels (g-i) are the corresponding CIGs at 18 km on the profile.

Good fitting of the data (Figure 10b) in spite of the inaccurately estimated ε demonstrates some nonuniqueness of the solution associated with limited data aperture. The perturbation of ε does not significantly affect the stacking amplitude for these data. The CIGs of the inverted and the correct models (Figure 15) are also very similar in the region sampled by the inversion (above the red line in Figure 14b). Thus, if the data quality (i.e., sufficient amplitude) is not present at large offsets, the best fitting (largest stacking amplitude) in each CRP gather is controlled only by V_{Po} and δ. Under this data condition, the additional degrees of freedom associated with the addition of ε make the multiparameter inversion ill posed.

An additional possible constraint is well data, when they are available. Bakulin et al. (2009) develop localized gridded anisotropic tomography, which combines surface seismic data with borehole measurements (acoustic logs or check-shot surveys). Well data can also be used in the CRP MVA. Agnihotri and McMechan (2007) develop parsimonious migration for VSP data; this framework can be extended to anisotropic media to be included in the CRP MVA.

Conventionally, V_{Po} and δ are estimated from well seismic data (Ferla and Cibin, 2009) and ε is calculated from NMO analysis by estimating the anellipticity coefficient η defined by Alkhalifah and Tsvankin (1995):

$$\eta = \frac{\varepsilon - \delta}{1 + 2\delta}. \tag{8}$$

However, seismic well data are sparse and, when available, not all the intervals in the well are sampled (Zhou et al., 2011). Thus, obtaining good estimations of V_{Po} and δ may lead to detecting the TTI media, even when no well data are available and when ε is not well estimated.

For data with noise with a signal-to-noise ratio (S/N) ~1.5, the accuracy of the p-value is affected because it is calculated by slant stacking the data; so noisy data may produce inaccurate p-values. The anomalous values at the edges of ϕ (Figure 11d) are caused by low sampling (Figure 12) that produces errors in the migration and so also in the estimation of the update of ϕ. However, the updated traveltimes fit the reflection moveouts very well (Figure 10c). An advantage of this methodology is that the reflection points are selected only from a reference common-offset section, and only significant reflections are picked. So it is straightforward to avoid reflections at noisy offsets. However, if the S/N decreases, the CRP MVA will be affected significantly because the p-values calculations may not be accurate (Hua and McMechan, 2001). Random noise will tend to cancel when the reflection moveout is coherent and so may not significantly affect the estimation of the stacking amplitude through the updated traveltime trajectories.

Resolution is determined by the separation of the time picks; it is only possible to obtain distributions of the anisotropy parameters that are smoothly varying between the time picks of the reference-offset section. Thus, the final inverted BP TI model (Figure 11) is a smoothed version of the correct solution (Figure 8). The anisotropic parsimonious depth migration in the CRP MVA gives an explicit estimation of reflector orientation and thus, of symmetry axis orientation for the BP TTI data (Figure 11d) because it is constrained to be normal to the reflector.

A viable strategy is to initially parameterize the model with a few widely spaced reflections that bound homogeneous regions, and then to use that result as the starting model for inversions that gradually allow us to have more reflections and to be more

heterogeneous. Conversely, the layer stripping reduces the number of variables to be solved for at each iteration and stabilizes the inversion by reducing the number of degrees of freedom.

As the algorithm uses wave amplitudes only indirectly (to define the P-wave reflection time trajectories) it is not necessary to preserve accurate amplitudes for field data preprocessing. However, the ideal data should contain only P-wave reflections. Thus, direct P- and S-waves, primary or converted S-waves, surface waves, and all coherent noise- and nonsource-generated waves should be muted or filtered prior to time picking, p calculation, and migration. The usual tapering of amplitudes at the offset and time edges of the data gathers during preprocessing is not necessary because the relatively small aperture of the parsimonious impulse response does not produce high-angle artifacts. For field data, the source wavelet and directivity also needs to be estimated, either a priori, or solving for it iteratively as part of the inversion.

The limitations in inversion for anisotropy parameters from time data can only be removed by fitting amplitude as well as time data (Chang and McMechan, 2009), but that is beyond the scope of the present paper. Another potential future application is to combine estimation of anisotropy parameters with a second inversion based on a fracture model, to estimate fracture properties such as crack density and fluid content, for reservoir characterization and monitoring.

CONCLUSIONS

To extend a previously developed isotropic algorithm to handle P-wave reflections from TTI media, we retain the same strategy and data flow, but need to redevelop each of the algorithm components; the ray tracing needs to be anisotropic, the parameterization needs to be expanded to contain V_{Po}, δ, ε, and the tilt angle ϕ, and phase and group velocities need to be calculated. We use the Newton method to improve convergence of the (iterative) solution of the phase angles and a nonlinear (parabolic) fitting in the gradient direction to find the next step in the ($\Delta\delta$, $\Delta\varepsilon$) plane in the iterative solution for δ and ε.

The tilt of the anisotropic symmetry axis ϕ is the most difficult parameter to estimate; we use the geologically realistic constraint that ϕ is perpendicular to the local reflector. Thus, it changes as the reflector position and orientation is changed by the migration at each iteration. Errors in ϕ affect the estimation of δ and ε if the error is $>5°$ and affect the estimation of V_{Po} as well as of ε and δ if the error is $>10°$.

For the simple case of a single TTI layer bounded at its bottom by a reflector containing flat and steep dips, and which is known to be homogeneous (so the inversion is for only one value of each of the four parameters), the inversion converges efficiently to the correct solution. In the BP model example, in which the model is gridded and variable from point to point, the range of propagation angles is not sufficient to allow estimation of ε; only angles near to the symmetry axis are recorded in the data, so only V_{Po} and δ can be recovered (and implicitly ϕ from the reflector orientations).

ACKNOWLEDGMENTS

We thank the sponsors of the University of Texas at Dallas Geophysical Consortium for supporting this project and the Texas Advanced Computing Center (TACC) for high-performance computing time. We thank BP for providing the 2D TTI data set. We also like to thank the Seismic Waves in Complex 3D Structures (SW3D) project from The Charles University of Prague for providing the ANRAY ray tracer, versions 4.5 and 4.7, used in this paper. Constructive comments by T. Alkhalifah and I. Pšenčík are much appreciated. This paper is contribution no. 1258 from the Department of Geosciences at the University of Texas at Dallas.

APPENDIX A

VELOCITY, TRAVELTIME, AND REFLECTION POINT PERTURBATIONS

Isotropic traveltime prediction

For isotropic media, the traveltime prediction (T) for incident angle θ_i is calculated by (Fei and McMechan, 2006a, 2006b)

$$T = \left[T_c + \frac{2\Delta l \cos(\theta_i)}{V}\right]\alpha, \tag{A-1}$$

where T_c is the two-way traveltime calculated by ray tracing for each source-receiver pair that forms the CRP gather, V is the velocity at (above) the reflection point, θ_i is the angle that the raypath makes with the normal to the reflector, α is the velocity ratio used to perturb the velocity model (which is allowed to vary only within some acceptable range), and Δl is the adjustment of the reflection point position in the direction normal to the local reflector orientation to keep the reference traveltime constant when calculating the perturbed traveltime curve ($\Delta l = R' - R$) in Figure A-1. The corresponding adjustments to the source and receiver positions are made in the following iteration. In an isotropic medium, θ_i is equal for the incident and reflected raypaths and Δl is given by

$$\Delta l = \left(\frac{V}{\alpha}\right)\frac{(t_{\text{ref}} - t_n)}{2\cos(\theta_r)}, \tag{A-2}$$

where t_{ref} is the reference time (picked from the reference common-offset gather), θ_r is the angle that the reference raypath makes with

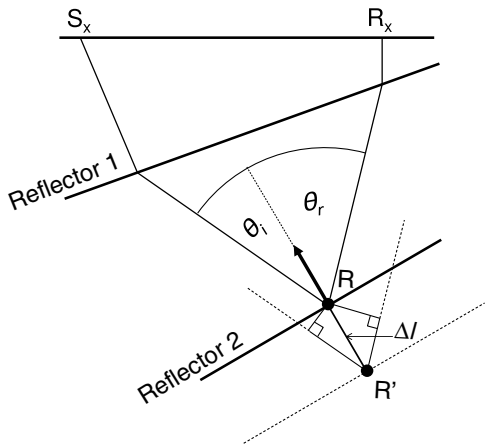

Figure A-1. Reference path geometry for reflection point analysis: S_x and R_x are the position of the source and the receiver, respectively, and Δl is the adjustment of the reflection point (R) so the traveltime remains unchanged at the reference offset when the velocity model is perturbed.

the normal to the local reflector, and t_n is the perturbed traveltime that corresponds to a change in the velocity by a factor α and is given by

$$t_n = t\alpha, \tag{A-3}$$

where t is the traveltime of the traveltime trajectory in CRP gathers.

Anisotropic traveltime prediction

For anisotropic (TI) media, the second term of equation A-1 is split because the incident and reflected angles are not equal unless the orientation of the axis of symmetry coincides with the local normal to the reflector. Thus, the anisotropic form of equation A-1 is

$$T = t_i + t_r + \Delta l\left(\frac{\cos(\theta_i)}{v_g(\theta_i)} + \frac{\cos(\theta_r)}{v_g(\theta_r)}\right) + t_s, \tag{A-4}$$

where t_i and t_r are the perturbed total incident and reflected traveltimes, respectively; v_g is the group velocity at (infinitesimally above) the reflection point; θ_i and θ_r are the corresponding group angles relative to the orientation of the local normal to the reflector at the reflection point (see Figure A-1); and t_s is a time shift that is applied to compensate for any systematic bias (Δt_m) between the picked traveltime (caused, for example, by a constant picking error) and the traveltime calculated from the raypaths that satisfy the time-imaging condition in the migration. Then, the updated traveltime coincides with the picked traveltime at the reference offset. t_s is given by

$$t_s = \Delta l_m\left(\frac{\cos(\theta_i)}{v_g(\theta_i)} + \frac{\cos(\theta_r)}{v_g(\theta_r)}\right), \tag{A-5}$$

where Δl_m is the (additional) adjustment of the reflection point in the direction of the local normal to the reflector (due to the above bias) given by

$$\Delta l_m = \Delta t_m\left(\frac{\cos(\theta_i)}{v_g(\theta_i)} + \frac{\cos(\theta_r)}{v_g(\theta_r)}\right)^{-1}. \tag{A-6}$$

The Δl_m is calculated for each CRP along the reference raypaths (in the migration) at each iteration of velocity adjustment.

Solving equation A-4 for Δl gives

$$\Delta l = [t_{\text{ref}} - (tp_i + tp_r)]\left(\frac{\cos(\theta_i)}{v_g(\theta_i)} + \frac{\cos(\theta_r)}{v_g(\theta_r)}\right)^{-1}, \tag{A-7}$$

where tp_i and tp_r are the perturbed traveltimes of the incident and reflected raypaths, in the reference raypath obtained in the migration, respectively and tp_i and tp_r are equal to t_i and t_r in equation A-4 only for the raypaths at the reference offset.

REFERENCES

Agnihotri, Y., and G. A. McMechan, 2007, Parsimonious migration of 3-C, 3D VSP data: Geophysics, **72**, no. 6, S205–S213, doi: 10.1190/1.2780221.

Alkhalifah, T., 1995, Gaussian beam depth migration for anisotropic media: Geophysics, **60**, 1474–1484, doi: 10.1190/1.1443881.

Alkhalifah, T., 1997, Seismic data processing in vertically inhomogeneous TI data: Geophysics, **62**, 662–675, doi: 10.1190/1.1444175.

Alkhalifah, T., 2011, Traveltime approximations for transversely isotropic media with an inhomogeneous background: Geophysics, **76**, no. 3, WA31–WA42, doi: 10.1190/1.3555040.

Alkhalifah, T., and P. Sava, 2010, A transversely isotropic medium with a tilted symmetry axis normal to the reflector: Geophysics, **75**, no. 3, A19–A24, doi: 10.1190/1.3409114.

Alkhalifah, T., and I. Tsvankin, 1995, Velocity analysis for transversely isotropic media: Geophysics, **60**, 1550–1566, doi: 10.1190/1.1443888.

Anderson, J., T. Alkhalifah, and I. Tsvankin, 1996, Fowler DMO and time migration for transversely isotropic media: Geophysics, **61**, 835–845, doi: 10.1190/1.1444008.

Bakulin, A., M. Woodward, D. Nichols, K. Osypov, and O. Zdraveva, 2009, Building TTI depth models using anisotropic tomography with well information: 79th Annual International Meeting, SEG, Expanded Abstracts, 4029–4033.

Barbosa, B., J. Costa, E. Gomes, and J. Schleicher, 2008, Resolution analysis for stereotomography in media with elliptic and anelliptic anisotropy: Geophysics, **73**, no. 4, R49–R58, doi: 10.1190/1.2917853.

Behera, L., and I. Tsvankin, 2009, Migration velocity analysis for tilted transversely isotropic media: Geophysical Prospecting, **57**, 13–26, doi: 10.1111/j.1365-2478.2008.00732.x.

Cai, J., Y. He, B. Wang, and M. Guo, 2009, TTI/VTI anisotropy parameters estimation by focusing analysis, Part I: Theory: 79th Annual International Meeting, SEG, Expanded Abstracts, 301–305.

Carcione, J. M., 2007, Wave field in real media: Wave propagation in anisotropic, anelastic, porous, and electromagnetic media: Elsevier.

Červený, V., 2001, Seismic ray theory: Cambridge University Press.

Chang, H., and G. A. McMechan, 2009, 3D 3-C full-wavefield elastic inversion for estimating anisotropic parameters: A feasibility study with synthetic data: Geophysics, **74**, no. 6, WCC159–WCC175, doi: 10.1190/1.3204766.

Charles, S., D. Mitchell, R. Holt, J. Lin, and J. Mathewson, 2008, Data driven tomographic velocity analysis in tilted transversely isotropic media: A 3D case history from the Canadian Foothills: Geophysics, **73**, no. 5, VE261–VE268, doi: 10.1190/1.2952915.

Crosson, R. S., 1976, Crustal structure modeling of earthquakes data: 1, Simultaneous least squares estimation of hypocenter and velocity parameters: Journal of Geophysical Research, **81**, 3035–3046, doi: 10.1029/JB081i017p03036.

Dellinger, J. A., 1991, Anisotropic seismic wave propagation: Ph.D. thesis, Stanford University.

Dewangan, P., and I. Tsvankin, 2006, Modeling and inversion of PS-wave moveout asymmetry for tilted TI media: Part I — Horizontal TTI layer: Geophysics, **71**, no. 4, D107–D121, doi: 10.1190/1.2210970.

Dong, Z., and G. A. McMechan, 1993, 3D prestack migration in anisotropic media: Geophysics, **58**, 79–90, doi: 10.1190/1.1443353.

Du, X., J. C. Bancroft, and L. R. Lines, 2007, Anisotropic reverse-time migration for tilted TI media: Geophysical Prospecting, **55**, 853–869, doi: 10.1111/j.1365-2478.2007.00652.x.

Farra, V., and I. Pšenčík, 2013, Moveout approximations for P- and SV-waves in VTI media: Geophysics, **78**, no. 5, WC81–WC92, doi: 10.1190/geo2012-0408.1.

Fei, W., and G. A. McMechan, 2006a, CRP-based seismic migration velocity analysis: Geophysics, **71**, no. 3, U21–U28, doi: 10.1190/1.2194530.

Fei, W., and G. A. McMechan, 2006b, 3D common-reflection point based seismic migration velocity analysis: Geophysics, **71**, no. 5, S161–S167, doi: 10.1190/1.2227523.

Ferguson, R., and G. F. Margrave, 1998, Depth migration in TI media by non-stationary phase shift: 68th Annual International Meeting, SEG, Expanded Abstracts, 1831–1834.

Ferla, M., and P. Cibin, 2009, Interval anisotropic parameter estimation in a least square sense application on Congo MTPN real dataset: 79th Annual International Meeting, SEG, Expanded Abstracts, 296–299.

Fletcher, X., R. P. Du, and P. J. Fowler, 2009, Reverse time migration in tilted transversely isotropic (TTI) media: Geophysics, **74**, no. 6, WCA179–WCA187, doi: 10.1190/1.3269902.

Gajewski, D., and I. Pšenčík, 1987, Computation of high-frequency seismic wavefields in 3-D laterally inhomogeneous anisotropic media: Geophysical Journal of the Royal Astronomical Society, **91**, 383–411, doi: 10.1111/j.1365-246X.1987.tb05234.x.

Gajewski, D., and I. Pšenčík, 1990, Vertical seismic profile synthetics by dynamic ray tracing in laterally varying layered anisotropic structures: Journal of Geophysical Research, **95**, 301–311, doi: 10.1029/JB095iB07p11301.

He, Y., and J. Cai, 2011, Anisotropic tomography for TTI and VTI media: 81st Annual International Meeting, SEG, Expanded Abstracts, 3923–3927.

Hua, B., and G. A. McMechan, 2001, Parsimonious 2D poststack Kirchhoff depth migration: Geophysics, **66**, 1497–1503, doi: 10.1190/1.1487095.

Hua, B., and G. A. McMechan, 2003, Parsimonious 2D prestack Kirchhoff migration: Geophysics, **68**, 1043–1051, doi: 10.1190/1.1581075.
Huang, T., S. Xu, J. Wang, G. Ionescu, and M. Richardson, 2008, The benefit of TTI tomography for dual azimuth data in Gulf of Mexico: 78th Annual International Meeting, SEG, Expanded Abstracts, 222–226.
Huang, T., S. Xu, and Y. Zhang, 2007, Anisotropy estimation for prestack depth imaging — A tomographic approach: 77th Annual International Meeting, SEG, Expanded Abstracts, 124–128.
Jiang, F., H. Zhou, Z. Zou, and H. Liu, 2009, 2D tomography velocity model building in tilted transversely isotropic media: 79th Annual International Meeting, SEG, Expanded Abstracts, 4024–4028.
Kumar, C., M. K. Sen, and R. J. Ferguson, 2004, Traveltime calculation and prestack depth migration in tilted transversely isotropic media: Geophysics, **69**, 37–44, doi: 10.1190/1.1649373.
Kumar, C., M. K. Sen, and R. J. Ferguson, 2008, Depth migration anisotropy analysis in time domain: Geophysical Prospecting, **56**, 87–94, doi: 10.1111/j.1365-2478.2007.00658.x.
Menke, W., 1984, Geophysical data analysis: Discrete inversion theory: Academic Press, Inc.
Oropeza, E. V., and G. A. McMechan, 2013, Anisotropic parsimonious prestack depth migration: Geophysics, **78**, no. 1, S25–S36, doi: 10.1190/geo2011-0408.1.
Postma, G. W., 1955, Wave propagation in stratified media: Geophysics, **20**,780–806, doi: 10.1190/1.1438187.
Ren, J., C. Gerrard, J. McClean, and M. Orlovich, 2005, Prestack wave-equation depth migration in VTI media: The Leading Edge, **24**, 618–620, doi: 10.1190/1.1946218.
Sarkar, D., and I. Tsvankin, 2004, Migration velocity analysis in factorized VTI media: Geophysics, **69**, 708–718, doi: 10.1190/1.1759457.
Sena, A. G., and M. N. Toksöz, 1993, Kirchhoff migration and velocity analysis for converted and nonconverted waves in anisotropic media: Geophysics, **58**, 265–276, doi: 10.1190/1.1443411.
Shewchuk, J. R., 1994, An introduction to the conjugate gradient method without the agonizing pain: Carnegie Mellon University.
Thomsen, L., 1986, Weak elastic anisotropy: Geophysics, **51**, 1954–1966, doi: 10.1190/1.1442051.
Tsvankin, I., 2005, Seismic signatures and analysis of reflection data in anisotropic media, *in* K. Helbig, and S. Treitel, eds., Elsevier: Handbook of geophysical exploration: Seismic exploration 29, 1–55.
Tsvankin, I., J. Gaiser, V. Grechka, M. var der Baan, and L. Thomsen, 2010, Seismic anisotropy in exploration and reservoir characterization: An overview: Geophysics, **75**, no. 5, 75A15–75A29, doi: 10.1190/1.3481775.
Tsvankin, I., and V. Grechka, 2011, Seismology of azimuthally anisotropic media and seismic fracture characterization: Geophysical Reference Series 17: SEG.
Vavryčuk, V., 2006, Calculation of the slowness vector from the ray vector in anisotropic media: Proceedings of the Royal Society of London, Series A: Mathematical, Physical and Engineering Sciences, **462**, 883–896, doi: 10.1098/rspa.2005.1605.
Wang, X., and I. Tsvankin, 2013, Ray-based gridded tomography for tilted transversely isotropic media: Geophysics, **78**, no. 1, C11–C23, doi: 10.1190/geo2012-0066.1.
Zhou, C., J. Jiao, S. Lin, J. Sherwood, and S. Brandsberg-Dahl, 2011, Multiparameter joint tomography for TTI model building: Geophysics, **76**, no. 5, WB183–WB190, doi: 10.1190/geo2010-0395.1.
Zhu, T., S. H. Gray, and D. Wang, 2007, Prestack Gaussian-beam depth migration in anisotropic media: Geophysics, **72**, no. 3, S133–S138, doi: 10.1190/1.2711423.